Development 135, 3881-3889 (2008) doi:10.1242/dev.022723

Arginyltransferase regulates alpha cardiac actin function, myofibril formation and contractility during heart development

Reena Rai[1], Catherine C. L. Wong[2], Tao Xu[2], N. Adrian Leu[1], Dawei W. Dong[3], Caiying Guo[4], K. John McLaughlin[1], John R. Yates, III[2] and Anna Kashina[1,5,*]

Post-translational arginylation mediated by arginyltransferase (Ate1) is essential for cardiovascular development and angiogenesis in mammals and directly affects myocardium structure in the developing heart. We recently showed that arginylation exerts a number of intracellular effects by modifying proteins involved in the functioning of the actin cytoskeleton and in cell motility. Here, we investigated the role of arginylation in the development and function of cardiac myocytes and their actin-containing structures during embryogenesis. Biochemical and mass spectrometry analyses showed that alpha cardiac actin undergoes arginylation at four sites during development. Ultrastructural analysis of the myofibrils in wild-type and *Ate1* knockout mouse hearts showed that the absence of arginylation results in defects in myofibril structure that delay their development and affect the continuity of myofibrils throughout the heart, predicting defects in cardiac contractility. Comparison of cardiac myocytes derived from wild-type and *Ate1* knockout mouse embryos revealed that the absence of arginylation results in abnormal beating patterns. Our results demonstrate cell-autonomous cardiac myocyte defects in arginylation knockout mice that lead to severe congenital abnormalities similar to those observed in human disease, and outline a new function of arginylation in the regulation of the actin cytoskeleton in cardiac myocytes.

KEY WORDS: Protein arginylation, Heart development, Actin, Post-translational modifications, Myofibrils, Cardiac muscle

INTRODUCTION

Protein arginylation is a poorly understood post-translational modification mediated by the arginyltransferase Ate1 (Balzi et al., 1990), which transfers arginine (Arg) from tRNA onto proteins (Kaji et al., 1963; Soffer, 1968; Takao and Samejima, 1999). Ate1 is encoded by a single gene that is highly conserved in evolution from yeast to human, and is expressed as one or more isoforms produced by alternative splicing in different mouse tissues (Kwon et al., 1999; Rai and Kashina, 2005; Rai et al., 2006). No other arginyl transferases have been identified in eukaryotic species to date. In yeast, the *Ate1* gene is not essential for cell viability, whereas *Ate1* knockout in mice results in embryonic lethality and severe defects in cardiovascular development and angiogenesis (Kwon et al., 2002). Multiple proteins are arginylated in vivo (Bongiovanni et al., 1999; Decca et al., 2006a; Decca et al., 2006b; Eriste et al., 2005; Fissolo et al., 2000; Hallak and Bongiovanni, 1997; Kopitz et al., 1990; Lee et al., 2005), including 43 different proteins isolated from various mouse cells and tissues (Wong et al., 2007).

Ate1 knockout mice die between E12.5 and E17, with large hemorrhages, impairment of embryonic angiogenesis, and severe heart defects that include underdeveloped myocardium, septation defects [ventricular and atrial septal defects (VSD and ASD)], and non-separation of the aorta and pulmonary artery [persistent truncus arteriosus (PTA)] (Kwon et al., 2002). The underlying molecular mechanisms and cell lineage(s) responsible for these defects are unknown. It has been hypothesized that some, or all, of these defects might be due to impaired embryonic cell migration during heart formation. VSD, ASD and PTA defects are often observed in mice with knockout of genes that affect the migration of cells of the neural crest lineage (Gitler et al., 2002) and cell adhesion (Conti et al., 2004; George et al., 1997; George et al., 1993; Tullio et al., 1997). Cells derived from *Ate1* knockout embryos display severe defects in lamella formation that result in impairment of directional migration along the substrate, linked to arginylation of beta actin, a ubiquitously expressed non-muscle actin isoform that plays a crucial role in lamella formation and non-muscle cell locomotion (Karakozova et al., 2006). However, whether the heart defects seen in *Ate1* knockout embryos are linked to impairments in cell migration during development, or whether additional cell-autonomous changes in the cells composing the heart contribute to the *Ate1* knockout phenotype, remains to be addressed.

It has recently been found that a number of proteins in embryonic and adult mouse tissues are arginylated (Wong et al., 2007). Among these, a prominent arginylation substrate is alpha cardiac actin (also known as cardiac alpha actin, Actc1), the major component of the myofibrils in the cardiac muscle, the arginylation of which is likely to affect myofibril development and function. It is likely that impairment of this arginylation in the *Ate1* knockout mouse would lead to defects in myofibril development that would be evident upon comparison of the hearts of wild-type and *Ate1* knockout embryos, shedding light on the molecular role of arginylation in heart development and myofibril function.

To address the question of whether *Ate1* knockout results in cell-autonomous changes in cardiac myocytes and whether arginylation plays a role in myofibril development and function, we characterized embryonic actin by gel fractionation and mass spectrometry and found that during development, alpha cardiac actin exists in a highly arginylated state and contains a total of four arginylated sites,

[1]Department of Animal Biology and [5]Mari-Lowe Center for Comparative Oncology, School of Veterinary Medicine, University of Pennsylvania, Philadelphia, PA 19104, USA. [2]The Scripps Research Institute, La Jolla, CA 92037, USA. [3]Florida Atlantic University, Boca Raton, FL 33431, USA. [4]Janelia Farm, Ashburn, VA 20147, USA.

*Author for correspondence (e-mail: akashina@vet.upenn.edu)

Accepted 6 October 2008

including two that were previously unknown. The four added arginines are likely to act in conjunction within the folded actin monomer to modulate actin polymerization and co-assembly with other myofibril proteins. Analysis of myofibril development at early stages of heart development, as well as between E12.5 and E14.5 when the phenotypic changes in *Ate1* knockout embryos become obvious, showed that lack of arginylation results in delayed myofibril formation and various structural defects in the myofibrils that suggest impairment in cardiac contractility. Studies of cardiac myocytes in culture support these conclusions and suggest that arginylation plays a key role in the functioning of cardiac myocytes. These results demonstrate cell-autonomous changes in cardiac myocytes that develop in response to *Ate1* knockout and suggest a key role of actin arginylation in the development and function of cardiac muscle in vivo.

MATERIALS AND METHODS

Ate1 knockout mice

Mice with deletion of exons 2-4 of *Ate1* were newly rederived using the targeting vector and strategy described by Kwon et al. (Kwon et al., 2002). PCR genotyping of mice and embryos used for heart and myocyte derivation was performed using a mixture of the three primers 5′-CTGTTCCA-CATACACTTCATTCTCAG-3′, 5′-GGTGCAAGTTCCTGTCTATT-3′ and 5′-AATTGGAGGGGGATAGATAAGA-3′ to detect products of 603 bp (wild-type allele) and 417 bp (knockout allele).

Actin fractionation and analysis

For two-dimensional gel analysis, whole E12.5 embryonic hearts were washed in PBS, flash frozen in liquid nitrogen, supplemented with 50 μl of 2× SDS sample buffer [5% SDS, 5% β-mercaptoethanol, 10% glycerol, 60 mM Tris (pH 6.8) (Burgess-Cassler et al., 1989)], homogenized by grinding and pipetting and boiled for 10 minutes for the subsequent electrophoretic fractionation. Complete dissolution of proteins was confirmed by centrifugation of the samples at 13,000 ***g*** for 15 minutes and visual confirmation that no pellet was present in the tube. Two-dimensional gel electrophoresis was performed by Kendrick Laboratories (www.kendricklabs.com) with SDS-boiled samples using carrier ampholines with isoelectrofocusing tube gels that enable isoelectrofocusing of samples prepared with SDS buffer as described (Anderson and Anderson, 1978). Spots corresponding to individual actin isoforms were excised from dried Coomassie-stained gels and analyzed by mass spectrometry as described (Karakozova et al., 2006; Wong et al., 2007) for protein identification and mapping of the arginylation sites.

For the analysis of the protein composition of the myofibrils (see Fig. S2 in the supplementary material), myofibril isolation was performed as previously described (Meng et al., 1996). In brief, individual E12.5 embryonic hearts were homogenized in 20 volumes (per weight) of buffer I (39 mM sodium borate, 35 mM KCl, 5 mM EGTA, 1 mM DTT, pH 7.1) and centrifuged at 1500 ***g*** for 12 minutes. The pellets were resuspended in 20 volumes of buffer II (39 mM sodium borate, 25 mM KCl, 1 mM DTT, pH 7.1) and centrifuged at 1500 ***g*** for 12 minutes. The pellets were further re-extracted for 30 minutes with Triton X-100 buffer (39 mM sodium borate, 25 mM KCl, 1 mM DTT, 1% Triton X-100, pH 7.1) and centrifuged at 1500 ***g*** for 12 minutes, followed by a wash with 20 volumes of suspension buffer (10 mM Tris, 100 mM KCl, 1 mM DTT, pH 7.1) and centrifugation at 1500 ***g*** for 30 minutes. The final pellets containing myofibrils were resuspended in 15 μl of 1× sample buffer and boiled for 15 minutes before loading on an SDS-PAGE gel.

Gel scanning and densitometry for determination of the percentages of arginylated actin and the myosin to actin ratio in the myofibril preparations were performed on inverted black and white images of gels, as shown in Fig. 1A, using the 'gray level' quantification in the Metamorph imaging software (Molecular Devices).

Electron microscopy

Whole mouse embryos at E9.5 and hearts excised from E12.5 and E14.5 mouse embryos were washed in PBS and fixed in 2.5% glutaraldehyde and 2% paraformaldehyde in buffer C (0.1 M sodium cacodylate, pH 7.4) overnight at 4°C, followed by two 10-minute washes in buffer C and post-fixation in 2% osmium tetroxide in buffer C. For staining, fixed embryos or hearts were washed twice for 10 minutes each in buffer C, once for 10 minutes in distilled water, incubated 1 hour at room temperature in a 2% aqueous solution of uranyl acetate and then washed twice for 10 minutes each in distilled water. For embedding, stained embryos or hearts were dehydrated by incubation for 10 minutes each in 50%, 70%, 80%, 90% and 100% ethanol, followed by two 5-minute incubations in propylene oxide (PO), overnight incubation in 1:1 PO:Epon (Poly/Bed 812, Polysciences), and then 1 day in 100% Epon. Epon-embedded embryos or hearts were kept for 2 days at 60°C for Epon polymerization, sectioned, stained with 1% uranyl acetate in 50% methanol and with a 2% (w/v) solution of bismuth subnitrite at 1:50 dilution, and then overlaid onto Formvar-coated grids for electron microscopy. Four embryos at E9.5 and four hearts at E12.5 (two wild-type and two knockout each) and six hearts at E14.5 (three wild-type and three knockout) were used for the measurements and observations shown in Figs 2-4 and in Fig. S3 in the supplementary material.

Cardiac myocyte derivation and beat measurements

For cardiac myocyte derivation, whole hearts from E12.5 embryos were washed with warm PBS, placed into 200 μl of prewarmed 1% trypsin in PBS and incubated at 37°C for ~5 minutes. After digestion, heart tissue was gently pipetted up and down until the large aggregates were broken apart, the cell suspension was diluted with 1 ml of DMEM:F10 culture medium supplemented with 10% FBS, centrifuged for 5 minutes at ~100 ***g***, resuspended in ~2 ml of the same medium, and plated onto 3.5-cm collagen-coated glass-bottom dishes (Matek). Cells were incubated overnight in culture for attachment and spreading.

For myocyte beat measurements, time-lapse videos of individual myocytes or islands were obtained over 1 minute at half-second intervals (120 frames) using phase-contrast 10×, 20× or 40× objectives and an Orca AG digital camera (Hamamatsu). In each video, beats of individual cells or isolated islands were measured by selecting a 10×10 pixel region in the area of the cell where the gray value (image intensity) displayed obvious changes during each contraction (as shown in Fig. 5C), and total gray value over time in this region was measured using Metamorph. Time intervals between the centers of gray value peaks, which were determined automatically after smoothing the baseline and scaling up the peaks, were used for frequency diagrams and for calculation of means and ratios as shown in Fig. 5. For measurement of calcium changes during beats, the medium in the dishes with cultured myocytes was supplemented with 2.5 μM cell-permeable Fluo-4 fluorescent calcium indicator dye (Invitrogen), followed by a 30-minute incubation for dye loading. Individual cells and islands were then placed into fresh medium and imaged by phase-contrast time-lapse over 25 seconds, acquired at four frames per second, followed by imaging of the same field in the fluorescent channel for the same time interval. Calcium change periodicity was measured by changes in light intensity (gray levels) in a 10×10 pixel region located in the center of a beating cell, and intervals between peaks were determined and compared with those obtained during phase-contrast imaging of the same cells for the correlation plot shown in Fig. 5D.

RESULTS

Alpha cardiac actin is arginylated in vivo on multiple sites

We recently found that actin is arginylated in vivo and that this arginylation regulates its key properties and functions in the actin cytoskeleton (Karakozova et al., 2006; Wong et al., 2007). One of the two actin isoforms shown to undergo arginylation is alpha cardiac actin, a key heart protein and the major component of the cardiac myofibrils. To address the question of whether alpha cardiac actin is arginylated during embryogenesis and to estimate the percentage of actin arginylated in vivo, we fractionated whole mouse hearts derived from E12.5 wild-type and *Ate1* knockout mouse embryos by 2D gel electrophoresis under a pH gradient that allows separation of actin isoforms (Fig. 1A), and identified the actin isoform composition of the individual spots by mass spectrometry.

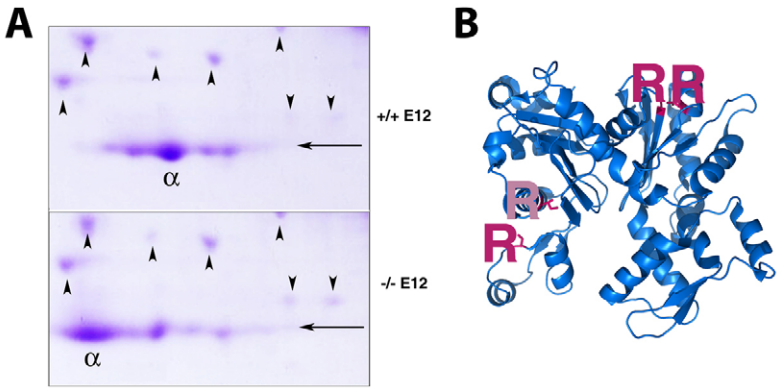

Fig. 1. Alpha cardiac actin is arginylated in vivo. (**A**) Areas of a Coomassie-stained 2D gel of protein samples obtained by fractionation of whole E12.5 mouse hearts from wild-type (+/+, top) and *Ate1* knockout (–/–, bottom) embryos under a shallow pH gradient (pH 4-8) to enable separation of individual actin isoforms. pH increases from left to right. Arrowheads indicate the position of spots that were used for the horizontal alignment of the two gels to enable observation of gel shifts of individual actin spots. Arrows indicate the position of the 43 kDa marker, equivalent to the molecular weight of intact alpha actin. α, the position of alpha cardiac actin as identified by mass spectrometry. (**B**) Three-dimensional structure of an alpha cardiac actin monomer (PDB identifier 1J6Z) with post-translationally arginylated sites (R) indicated in pink within the blue actin backbone. The site indicated in pale pink, for which the mass spectrum is not shown, will be described elsewhere.

Actin isoforms (α, β, γ) are over 99% identical to each other, with small variations in amino acid composition that lead to shifts in isoelectric point (Otey et al., 1987; Otey et al., 1986; Rubenstein and Spudich, 1977; Vandekerckhove and Weber, 1978) that can be seen when fractionation is performed under a shallow pH gradient (pH range 4-8); alpha actin is the most acidic and appears as the leftmost spot(s) on such gels.

Whereas adult hearts express predominantly alpha cardiac actin, a greater variety of actin isoforms are expressed simultaneously during embryogenesis (Hayward and Schwartz, 1986; Otey et al., 1988; Sassoon et al., 1988), resulting in multiple spots in the appropriate pH range of the gel in addition to the major, alpha actin spot (Fig. 1A, top panel). Comparison of the actin spot composition of wild-type and *Ate1*$^{-/-}$ E12.5 hearts revealed a striking change in the position of the major isoform spot (α, Fig. 1A), which was significantly shifted to the more acidic end of the range (left), consistent with the loss of several positive charges. Since Arg is highly positively charged, and addition of Arg to proteins is expected to result in a shift in the isoelectric point towards the basic range, the gel shift observed between wild-type and *Ate1* knockout hearts is consistent with the addition of several Arg residues to the wild-type actin molecule. To confirm this, we analyzed the major actin spots, excised from the gels similar to those shown in Fig. 1A, by mass spectrometry, using a high accuracy LTQ-Orbitrap MS instrument and a database search algorithm to look for the addition of an extra Arg to the N-terminus of the peptides (Wong et al., 2007). Although the sequence coverage of gel-excised spots was significantly lower than for samples analyzed in solution, analysis of actin spots excised from several different gels resulted in the identification of two previously unknown arginylation sites, one at isoleucine 87 (in pale pink on the diagram in Fig. 1B; this site will be described in detail elsewhere), and one at glycine 152 (for the mass spectrum of the corresponding peptide, see Fig. S1 in the supplementary material). Remarkably, although both sites are located far from the N-terminus and are expected to require a preceding proteolytic cleavage to become accessible for arginylation, they were found in actin excised from an intact 2D gel spot (43 kDa), suggesting that the molecule remained together during SDS-PAGE. The chemistry behind this reaction and the processing that leads to intrachain cleavage and arginylation without destroying the integrity of the molecule will be described elsewhere.

Mapping of all four of the identified arginylated sites onto the actin 3D structure [PDB identifier 1J6Z (Otterbein et al., 2001)] revealed that all these sites are accessible on the surface of the folded subunit, but some sites might not be accessible after polymerization (the two sites on the top), suggesting that modification of these sites could occur after subunit folding but before incorporation into the polymer. The sites are located pairwise on the actin surface, with two arginylated residues directly facing each other in the folded structure (Fig. 1B, in pink within the blue chain of the actin backbone). Insertion of Arg into these positions would be predicted to affect the molecular structure of the actin monomer, its polymerization properties and interaction with other proteins in the myofibril.

Estimation by gel densitometry of the arginylation-dependent gel shifts of the alpha cardiac actin shown in Fig. 1A suggests that as much as 40% of the total embryonic heart actin, and 50% of the alpha actin, is arginylated in vivo. Thus, alpha cardiac actin in embryonic hearts exists in a highly arginylated state and *Ate1* knockout results in the abolishment of actin arginylation, which is expected to result in significant structural and functional changes in the actin molecule.

Arginylation regulates myofibril assembly, structure and continuity throughout the heart

To test whether arginylation knockout results in defects in myofibril structure and/or assembly at the onset and during the progression of the phenotypic changes in *Ate1*$^{-/-}$ embryos, we analyzed sections of fixed hearts derived from E12.5 and E14.5 wild-type and knockout littermate embryos by electron microscopy. These stages were chosen because at E12.5, *Ate1*$^{-/-}$ embryos appear to be phenotypically normal such that only the most significant early myofibril defects, if any, are expected to be seen, whereas at E14.5, most knockout embryos look grossly abnormal and some of them start to die, so any myofibril defects in response to the *Ate1* knockout would be highly prominent at this point.

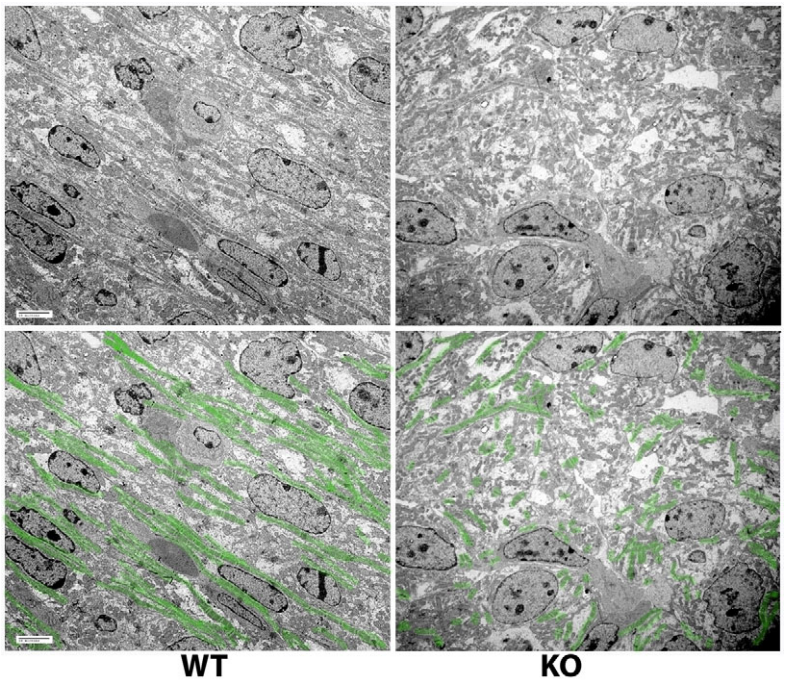

Fig. 2. *Ate1* knockout results in the delayed development and the disorganization of cardiac myofibrils. Electron microscopy images of sections of wild-type (WT, left column) and knockout (KO, right column) E14.5 mouse hearts at 2500× magnification. The same images are shown in the bottom row, but with myofibrils highlighted in green. In the wild type at E14.5, myofibrils are prominent and are oriented along the axis of the heart muscle. In the knockout at the same stage, myofibrils are much less abundant and difficult to trace over continuous distances, suggesting a defect in overall myofibril organization and cardiac contractility. Scale bars: 10 μm.

Examination of the heart structure at lower magnification (×250, not shown) confirmed that *Ate1* knockout hearts, consistent with previously reported observations, had thin walls owing to the reduced size of the compact zone of the myocardium (Kwon et al., 2002). Higher magnification views of the large areas of the heart (×2500, Fig. 2) revealed significant structural changes in *Ate1* knockout hearts compared with their wild-type counterparts. In wild-type hearts, the development of highly organized, continuous myofibrils progressed robustly from E12.5 to E14.5, whereas in the *Ate1* knockout, this development appeared to be delayed, resulting in scarce, disorganized myofibrils, the continuity of which could not be traced through multiple myocytes (Fig. 2, right). The prominence and severity of these defects varied between individual embryos and across the heart areas analyzed, but all the hearts used in this analysis displayed similar trends. In the most severe cases, as observed in hearts taken from E14.5 embryos with prominent phenotypic changes [reduced size, paleness and hemorrhages as described by Kwon et al. (Kwon et al., 2002)], the myofibril structure and connections between the myocytes were disrupted, suggesting that such hearts would be unlikely to function normally. Overall, the observed changes suggested that *Ate1* knockout resulted in the delayed development and the disorganization of the myofibrils and disruption of their continuity between interconnected cells, all of which are predicted to affect contractility within the heart muscle.

To address the question of whether such global changes in myofibril layout are accompanied by ultrastructural changes in the myofibrils, we first compared the protein composition of the myofibrils isolated from wild-type and *Ate1* knockout hearts at E12.5. Although no consistent changes were detected, the preparations from knockout hearts were somewhat more variable and the ratio of myosin to actin, as quantified by gel densitometry, was slightly lower than in the wild type (see Fig. S2 in the supplementary material), suggesting that at this stage the myofibrils in the knockout hearts might be more structurally unstable than in the control. This instability might be due to specific structural changes in the myofibrils themselves, or to the general onset of heart failure resulting from *Ate1* knockout.

We next analyzed higher magnification images of the sarcomeres and intercalated disks in wild-type and mutant hearts (Figs 3 and 4). Several structural features of the myofibrils and intercalated disks were evaluated quantitatively, including sarcomere length and Z-band thickness (as measures of sarcomere structure, Fig. 3), the angle of myofibrils and their component filaments at intercalated disks (a measure of myofibril continuity throughout the heart), and cell-cell distance at intercalated disks (a measure of heart muscle integrity) (Fig. 4). In addition, the general appearance of the myofibrils was evaluated. Only the fully developed, structurally distinct myofibrils were evaluated in both conditions, so the analysis presented in Figs 3 and 4 does not reflect any measure of the rate of myofibril development, which was difficult to evaluate owing to possible variation in the area of the heart muscle that was used for sectioning in each heart.

Several prominent defects were observed in the myofibrils with the progression of *Ate1* knockout-related phenotypic changes. At E12.5, most of the sarcomeres and Z-bands in fully developed myofibrils appeared normal, whereas at E14.5 the hearts with more severe defects showed sarcomere collapse (Fig. 3), with a progressive decrease in the length of individual sarcomeres and diffusion of the Z-bands in a manner that suggested disconnection of the Z-bands from the myofibrils. Some of the myofibrils became wavy and uneven, with prominent loss of Z-bands and fraying of the filaments out of the sarcomeres (Fig. 3D, bottom image). A variety of other structural abnormalities were observed, including myofibril branching at Z-bands, asymmetric sarcomeres with a different density of filaments on the two sides of the same sarcomere (Fig. 3E), and patchy or missing Z-bands (not shown; also observed in the wild type, but more often seen in the knockout).

Defects were also seen at intercalated disks, which serve as the sites of connection of the myofibrils between neighboring myocytes and ensure myofibril continuity throughout the heart. First, in most of the observed cases, including E12.5 hearts in which other ultrastructural features were apparently normal, the filaments within a myofibril approached the intercalated disk at different angles, resulting in tapered (E12.5 and E14.5), frayed and/or disoriented

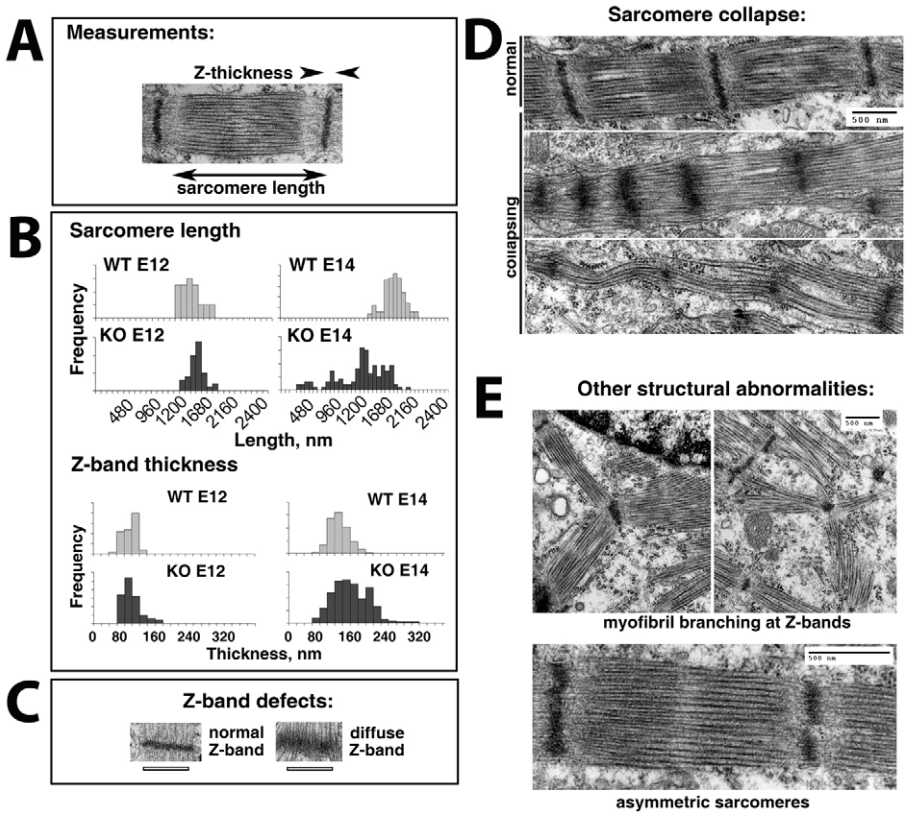

Fig. 3. *Ate1* knockout results in defects in the sarcomeric structure of cardiac myofibrils. (**A**) Wild-type sarcomere illustrating parameters measured. (**B**) Frequency distribution of sarcomere length and Z-band thickness in wild-type (WT) and knockout (KO) mouse hearts at E12.5 (E12) and E14.5 (E14). In wild-type and mutant E12.5 hearts, both sarcomere length and Z-band thickness are relatively constant, with small variations due to differences in the contractile state of individual myocytes. In knockout hearts at later stages (E14.5), the frequency distribution of both parameters becomes wider, suggesting disorganization of the sarcomeres. (**C**,**D**) Defects in Z-band thickness (C) and sarcomere length (D). Average sarcomere lengths (± s.d.) were 1389 ± 141 nm (WT E12, *n*=27), 1490 ± 101 nm (KO E12, *n*=39), 1682 ± 116 (WT E14, *n*=116) and 1179 ± 199 (KO E14, *n*=124). Average Z-band thicknesses were 86 ± 19 nm (WT E12, *n*=27), 87 ± 23 nm (KO E12, *n*=39), 120 ± 23 (WT E14, *n*=116) and 142 ± 36 (KO E14, *n*=124). (**E**) Examples of other defects in myofibril structure seen in *Ate1* knockout hearts, including myofibril branching at Z-bands and asymmetric sarcomeres, in which the density of the filaments on the two sides is markedly different. Scale bars: 500 nm.

(E14.5) or disconnected (i.e. missing myofibrils on one side of the intercalated disk, E14.5) morphology (Fig. 4E, top three images) that suggested structural and functional discontinuity of the myofibrils between myocytes. In more severe cases, disruption of the intercalated disks themselves was observed (Fig. 4E, bottom image). All these changes suggest contractility defects and disconnection between individual myocytes in the myocardium.

To further address the question of whether the myofibril defects in *Ate1* knockout hearts are accompanied by a delay in myofibril development, we analyzed myofibril ultrastructure in the hearts of *Ate1* knockout embryos at earlier stages (E9.5). At these stages, no gross phenotypic changes in *Ate1* knockout embryos have been reported, despite the fact that *Ate1* expression is at its peak (Kwon et al., 2002) and therefore Ate1-related developmental defects should already be initiated. Consistent with the earlier studies (Kwon et al., 2002), no gross morphological changes were seen in E9.5 *Ate1* knockout hearts as compared with the control. Both types of heart contained prominent myofibrils as well as disarrayed myofibril-like structures, indicating that at this stage the development of the heart muscle is still ongoing. Comparison of the 'least developed' and the 'most developed' myofibrils seen in both types of embryo at this stage (see Fig. S3 in the supplementary material) suggested that in *Ate1* knockout mice, myofibrils were thinner than in the wild type and contained a smaller amount of prominent Z-bands. To quantify this defect, we measured the length of the Z-bands (a measure of the myofibril thickness and therefore of the extent of myofibril development) in both types of heart at E9.5 and E14.5 and compared the distributions of Z-band lengths in the wild type and knockout at these stages. Although the length of the Z-bands increased considerably at later developmental stages, they were consistently shorter in the *Ate1* knockout than in the wild type. This effect was especially prominent at E9.5, when the peak Z-band lengths were ~300 nm in the wild type and ~200 nm in the *Ate1* knockout (see Fig. S3 in the supplementary material). These results suggest that in addition to the ultrastructural changes in the myofibrils seen at later stages, myofibril development is also delayed in *Ate1* knockout embryos.

Thus, *Ate1* knockout results in delayed myofibril development, changes in sarcomere structure and in a discontinuity of the myofibrils throughout the heart.

Arginylation regulates cardiac myocyte contractility in culture

To address the question of whether the observed myofibril defects result in changes in the contractility of the cardiac myocytes, we isolated myocytes from E12.5 wild-type and *Ate1* knockout embryos and observed their spontaneous contractility in a tissue culture dish. In both cultures, two types of cells were present: flat, well-spread polarized fibroblasts, and less well-spread, mostly hexagonally shaped myocytes that often formed small islands with two or more cells clustering together. Most of the cells with myocyte morphology exhibited spontaneous contractility during the first 2-3 days in culture (the time interval used for the analysis). Fewer myocytes appeared to be beating in the knockout cultures, but this effect was not quantified because of the lack of criteria for a formal quantitative distinction between myocytes and non-myocyte cells in culture. After a few days in culture, most of the *Ate1* knockout myocytes ceased to beat, whereas in the control cultures many more cells were still beating (suggesting that the wild-type cells are 'sturdier' in these culture conditions and/or more capable of continuous beating), but because by that time the culture dish was usually overgrown with fibroblasts and cells of the myocyte morphology were difficult to identify, this effect was not quantified.

To measure the beating rates of individual myocytes and myocyte islands in culture, we made time-lapse movies of beating myocytes taken at half-second intervals over the course of 1 minute in both

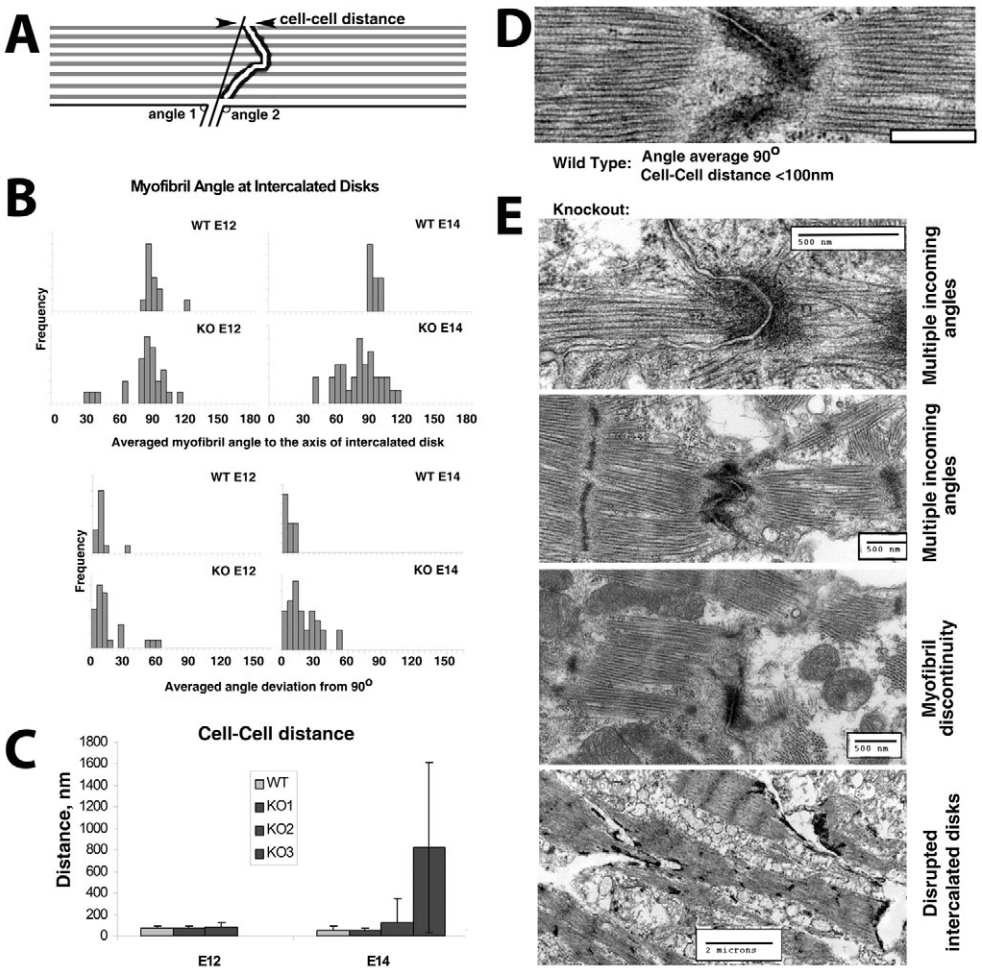

Fig. 4. *Ate1* knockout results in defects in myofibril continuity at intercataled disks. (**A**) Illustration of the structural parameters measured. (**B**) Frequency distribution of average myofibril angle at each intercalated disk (above) and deviation of this angle from 90° (below). (**C**) Cell-cell distance averaged for all wild-type mouse hearts together (light-gray bars) and for individual knockout hearts (dark-gray bars), sorted by embryo age. As the severity of the knockout phenotype progresses, the average cell-cell distance, as well as the standard deviation between distances in a single heart, increase, as seen at E14 for the three KO hearts shown. (**D,E**) Examples of intercalated disks in the wild type (D) and knockout (E). Abnormalities at intercalated disks included disorganization of the myofibrils resulting in angle deviations from 90° for incoming filaments (E, top two images), myofibril asymmetry on the two sides of the intercalated disk (E, the middle two images), and disruption of the cell-cell contacts at intercalated disks (E, bottom). Scale bars: 500 nm in D; 500 nm in E, except for bottom image at 2 μm.

cultures during the first 2 days after isolation, and measured the light intensity changes in phase-contrast time-lapse images over time (for the normalized plots of gray level changes over time for individual wild-type and knockout cells or islands, see Figs S4 and S5 in the supplementary material). As this relatively low sampling rate might have precluded us from measuring the actual beating rate at higher frequencies [>60 beats per minute (bpm)], we also manually calculated the number of cells beating at high frequency, and the number of cells displaying visibly irregular beating patterns, i.e. variable intervals and strength between individual beats (Fig. 5 and see Figs S4 and S5 in the supplementary material).

In both cultures, there was a wide range in the beating frequency of individual cells and islands and in the regularity of beats (for wild-type and knockout beating curves, see Figs S4 and S5 in the supplementary material). However, whereas in the wild-type cultures many cells were beating regularly and at a fairly slow rate (3-20 bpm, Fig. 5 and see Fig. S4 in the supplementary material), in the knockout cultures a considerable number of cells beat at high frequency (>20 bpm, Fig. 5 and see Fig. S5 in the supplementary material), elevating the mean bpm by a statistically significant number (Fig. 5A). The range in bpm observed in individual cells or islands displayed a somewhat wider distribution in the knockout cultures, but the difference was not statistically significant (not shown). However, the percentage of cells beating at high frequency and of cells with visible irregularities in their beating curves, from manual counting of the curves shown in Figs S4-S6 (see Figs S4-S6 in the supplementary material), was significantly higher in the *Ate1* knockout cells than in the wild type (Fig. 5A). In addition, by visual observation, knockout cells and islands appeared to contract more locally, with variations throughout the cell areas, suggesting local 'twitching' rather than a cell-wide contraction, consistent with the defects seen in myofibril continuity at the ultrastructural level. Although the effect was not quantified, these observations suggest that the increased occurrence of high frequency beats in the knockout cultures could reflect an abnormal, fibrillating behavior of the cells.

To confirm that the physical beating frequency measured in our experiments correlates with the changes in intracellular Ca^{2+}, we measured calcium waves (using Fluo-4 Ca^{2+} vital dye) and physical beats (using light intensity measurements of phase-contrast images) in the same cells and/or islands and plotted the correlation between the two measurements (Fig. 5D, see Fig. S6 in the supplementary material for the original curves). We found that in most wild-type and knockout cells, beats and calcium waves showed a good correlation, suggesting that the changes in the beating frequency of the knockout cells, despite their origin in structural defects in the myofibrils, were still tied into calcium-dependent regulation. To minimize the UV exposure for live cells in culture, these measurements were performed at a higher sampling rate (four frames per second over 25 seconds), resulting in an elevated average bpm for both cell types (not shown) and in an elevated ratio of beating frequency between wild type and knockout, as compared with those measured in the previous set of experiments (Fig. 5A and Fig. S6 in the supplementary material). This difference suggested that the earlier measurements, taken at a lower sampling rate, might

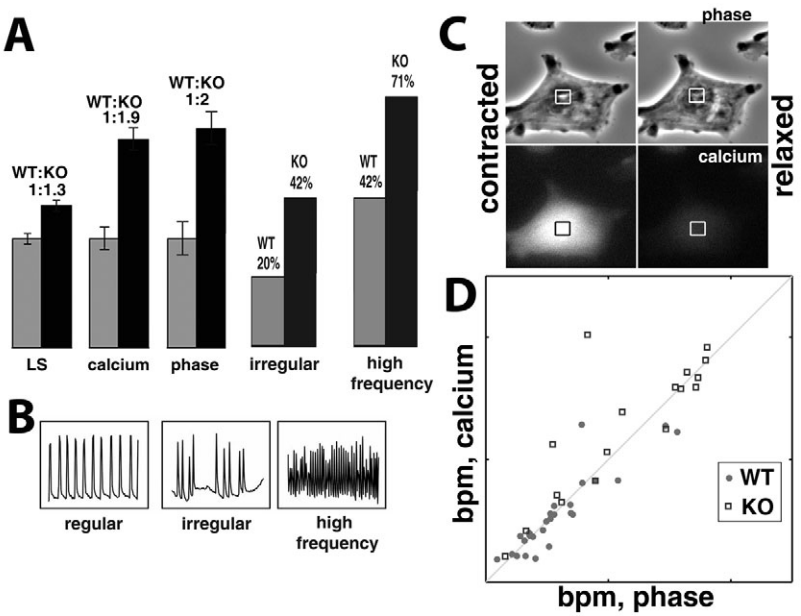

Fig. 5. *Ate1* knockout results in defects in cardiac myocyte beating patterns. (**A**) Comparison of mean beats per minute (bpm), percentage of cells beating at high frequency, and percentage of cells with visible irregularities in the beating pattern between wild-type (WT) and knockout (KO) cultured myocytes derived from E12.5 embryonic mouse hearts. Calculations were made for 164 WT and 233 KO cells/islands for the left-most set of bars at low sampling rate (LS, two frames per second), 28 WT and 17 KO cells/islands for the next two sets of bars [calcium and phase, sampled at four frames per second for the same cell/islands in fluorescence (calcium) channel and phase-contrast], and 194 WT and 250 KO cells for the two right-hand sets of bars (irregular and high frequency). For images of individual beating curves, see Figs S4-6 in the supplementary material. (**B**) Examples of beating frequency curves, which were considered as regular, irregular or high frequency during manual calculation of the curves shown in Figs S4-S6 (see Figs S4-S6 in the supplementary material) to derive the percentages shown in A. (**C**) Illustration of how beat and calcium waves were measured from the total 'gray level' in a region (square) of the beating cell that showed the most obvious changes (usually, the center). (**D**) Correlation plot between the physical beats observed in phase-contrast (*x*-axis) and calcium changes over time in the same cells (*y*-axis). For the most part, beats are correlated with calcium waves in both WT and KO cultures. For beating curves obtained by imaging of the same cells by phase-contrast and Fluo-4 calcium fluorescence, see Fig. S6 in the supplementary material.

not have reflected the real beating frequencies of the cultured myocytes. The rates detected in our studies are similar to those reported by other researchers studying myocyte beating in culture, but because mouse hearts in vivo beat at a much higher frequency [over 300 bpm (Mai et al., 2004)], it is possible that sampling rates in time-lapse imaging of cultured cells preclude accurate measurement of the beating rate. For this reason, actual bpm values were not used in our analysis, and only the bpm ratios between wild-type and knockout cultures are shown.

Thus, in agreement with our ultrastructural data, we find that *Ate1* knockout results in changes in the contractility and beating patterns of cardiac myocytes, suggesting corresponding changes in cardiac contractility in vivo.

DISCUSSION

Our study demonstrates that knockout of the arginyltransferase Ate1 leads to cell-autonomous defects in cardiac myocytes that develop during embryogenesis, affecting myofibril development and structure, myocardium integrity and myocyte contractility. Although it was known that *Ate1* knockout results in significant defects in heart development and in a reduced number of cells composing the heart walls, this is the first demonstration that some of the Ate1-regulated defects are directly associated with defects in the cells that compose the myocardium and are responsible for heart contractility.

We have previously shown that two actin isoforms, beta and alpha cardiac, are arginylated in vivo (Karakozova et al., 2006; Wong et al., 2007), and both isoforms are present in the developing heart. In this study, we identify two new sites of arginylation on alpha cardiac actin and provide a possible functional correlation between alpha actin arginylation and myofibril development and function. Our data suggest that an extremely high percentage of cardiac actin (~50%) is arginylated, supporting the proposal that actin arginylation is crucial for myofibril integrity. It has been shown previously that substitution of alpha cardiac actin with the gamma enteric muscle isoform (presumed to be non-arginylated) leads to altered mechanochemical properties of myofibrils isolated by detergent extraction of the heart muscle (Martin et al., 2002). Although gamma enteric smooth muscle actin could, hypothetically, become partially arginylated during this substitution, this finding is, overall, consistent with our data indicating that the actin arginylation state and the N-terminal actin sequence are important for myofibril function. Furthermore, our data suggest a direct role of arginylation in the regulation of actin function during myofibril assembly and heart development.

Two of the four arginylated sites were identified in actin polypeptides of intact size isolated from an SDS-PAGE gel, suggesting that these modifications exist within the intact, folded actin molecule that maintains its integrity during SDS-PAGE, and that they do not result in protein degradation or disassembly. The chemistry and enzymology of this reaction remain to be studied. The position of the arginylation sites in the actin 3D structure (Fig. 1B) suggests that arginylation of one, or more, of these sites would significantly alter actin polymerization properties and its ability to associate with other subunits during polymerization. Since the

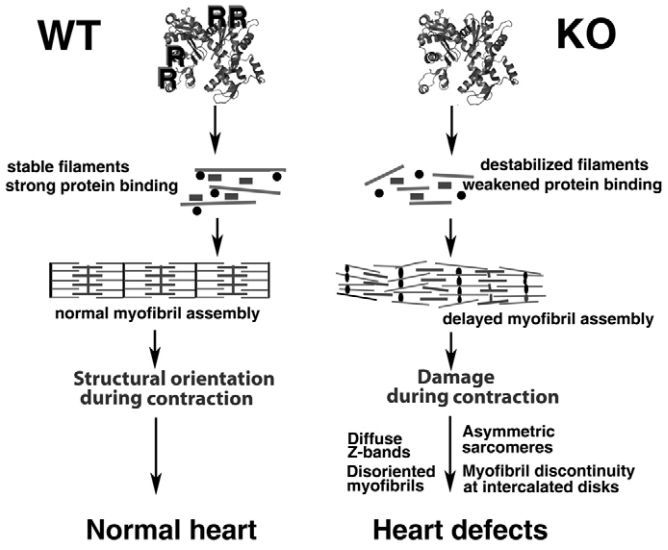

Fig. 6. Model of the regulation of myofibril assembly and function by arginylation. In wild-type (WT) mice, arginylated actin assembles into stable filaments and eventually into normal myofibrils. In the *Ate1* knockout, non-arginylated actin forms destabilized filaments, resulting in delayed myofibril development and profound structural defects.

arginylated (Ate1-positive) state of actin is the wild-type state, it is logical to assume that the absence of arginylation would result in the reduction of the ability of actin monomers to polymerize and/or interact with other actin-binding proteins, probably by the abolishment of Arg residues from key positions within the molecule.

Our findings that myofibril development is delayed from as early as E9.5 suggest that phenotypic changes in the *Ate1* knockout begin much earlier than previously reported. It is conceivable that underdeveloped myofibrils, forced to contract under duress during growth and development of the embryo, become more and more abnormal as development progresses. Such strain-dependent progression would also explain the variability of the myofibril defects in the *Ate1* knockout. Indeed, thicker, better developed myofibrils can endure longer, whereas thinner myofibrils disintegrate faster, leading to a variety of phenotypes both in the whole embryos and in individual myofibrils.

The timing of the myofibril defects seen in our study is consistent with the timing of other phenotypic changes in *Ate1* knockout mice that become apparent after E12.5, closer to E14.5. Whereas some of the defects described in the current work (disruption of intercalated disks) might constitute secondary defects resulting from the loss of heart integrity, possibly preceding death, others (myofibril disorganization, sarcomere collapse and Z-band diffusion) are likely to be primary defects due to the lack of arginylation of the major structural components of the myofibrils. Since a prominent peak of *Ate1* expression is observed at E8-9, after which *Ate1* expression declines, and as the phenotypic changes take another 3-4 days to develop (Kwon et al., 2002), it is conceivable that E8-9 mark the time in development when a substantial amount of myofibril proteins are arginylated and stocked up for further use. Actin is a good candidate for this type of regulation because it is a highly abundant, highly stable protein and a major structural component of the myofibrils that, as we have shown, is arginylated in embryogenesis to a significant extent. However, other proteins might also undergo similar regulation.

Among the current models of myofibril assembly during development, the favored model suggests their formation from premyofibrils by association of cytoplasmic actin filaments into minisarcomeres that later align into nascent myofibrils and further mature into myofibrils (LoRusso et al., 1997; Rhee et al., 1994; Sanger et al., 2000; Sanger et al., 2005). Lack of arginylation of actin and other myofibril components could conceivably affect one or more stages in this process, by slowing the polymerization of the initial actin filaments, enforcing their abnormal aggregation instead of normal association, or affecting their interaction with other key proteins that form the core of the myofibril structure (myosin II, capZ, alpha actinin, troponins, tropomyosin and others). In addition to alpha cardiac actin, our previous work showed that talin (which participates in the membrane association of premyofibril complexes), as well as spectrin and filamin (which are generally responsible for the assembly of actin-containing structures), are also targets for arginylation in vivo (Wong et al., 2007). We believe that a combination of these factors leads to a delay in myofibril assembly (Fig. 6), resulting in the formation of fewer myofibrils in the *Ate1* knockout hearts than in the control at the same embryonic stage. Since these myofibrils receive the same contractility signals as in the wild-type heart (as follows from our data, Fig. 5D), underdeveloped myofibrils under stress are more likely to develop structural abnormalities, eventually leading to their collapse and disintegration.

Our studies predict that cell-autonomous regulation of cardiac myocytes by arginylation is essential for myofibril stability, heart integrity and for the mechanical continuity of contraction throughout the myocardium. Changes in these processes constitute the underlying causes of congenital heart abnormalities and heart disease in humans. The study of their regulation by arginylation is an emerging field that promises to uncover new molecular mechanisms of heart development and function in normal physiology and disease.

We thank Neelima Shah and Ray Meade for heart sectioning and assistance with electron microscopy; Dr Roberto Dominguez for help with actin structure analysis and the preparation of Fig. 1B; Jon Johansen and the staff of Kendrick Laboratories for 2D gel electrophoresis; Dr Bruce Freedman for helpful suggestions on calcium imaging; Drs Howard Holtzer, Clara Franzini-Armstrong, John Murray, members of the Pennsylvania Muscle Institute and A.K.'s lab for helpful discussions; and Drs Sougata Saha and Satoshi Kurosaka for critical reading of the manuscript. This work was supported by NIH grant 5R01HL084419 and awards from WW Smith Charitable Trust and Philip Morris Research Management Group to A.K. and NIH P41 RR011823 to J.R.Y.

Supplementary material

Supplementary material for this article is available at
http://dev.biologists.org/cgi/content/full/135/23/3881/DC1

References

Anderson, N. G. and Anderson, N. L. (1978). Analytical techniques for cell fractions. XXI. Two-dimensional analysis of serum and tissue proteins: multiple isoelectric focusing. *Anal. Biochem.* **85**, 331-340.

Balzi, E., Choder, M., Chen, W. N., Varshavsky, A. and Goffeau, A. (1990). Cloning and functional analysis of the arginyl-tRNA-protein transferase gene ATE1 of Saccharomyces cerevisiae. *J. Biol. Chem.* **265**, 7464-7471.

Bongiovanni, G., Fissolo, S., Barra, H. S. and Hallak, M. E. (1999). Posttranslational arginylation of soluble rat brain proteins after whole body hyperthermia. *J. Neurosci. Res.* **56**, 85-92.

Burgess-Cassler, A., Johansen, J. J., Santek, D. A., Ide, J. R. and Kendrick, N. C. (1989). Computerized quantitative analysis of coomassie-blue-stained serum proteins separated by two-dimensional electrophoresis. *Clin. Chem.* **35**, 2297-2304.

Conti, M. A., Even-Ram, S., Liu, C., Yamada, K. M. and Adelstein, R. S. (2004). Defects in cell adhesion and the visceral endoderm following ablation of nonmuscle myosin heavy chain II-A in mice. *J. Biol. Chem.* **279**, 41263-41266.

Decca, M. B., Bosc, C., Luche, S., Brugiere, S., Job, D., Rabilloud, T., Garin, J. and Hallak, M. E. (2006a). Protein arginylation in rat brain cytosol: a proteomic analysis. *Neurochem. Res.* **31**, 401-409.

Decca, M. B., Carpio, M. A., Bosc, C., Galiano, M. R., Job, D., Andrieux, A. and Hallak, M. E. (2006b). Post-translational arginylation of calreticulin: a new isospecies of calreticulin component of stress granules. *J. Biol. Chem*. **282**, 8237-8245.
Eriste, E., Norberg, A., Nepomuceno, D., Kuei, C., Kamme, F., Tran, D. T., Strupat, K., Jornvall, H., Liu, C., Lovenberg, T. W. et al. (2005). A novel form of neurotensin post-translationally modified by arginylation. *J. Biol. Chem.* **280**, 35089-35097.
Fissolo, S., Bongiovanni, G., Decca, M. B. and Hallak, M. E. (2000). Post-translational arginylation of proteins in cultured cells. *Neurochem. Res.* **25**, 71-76.
George, E. L., Georges-Labouesse, E. N., Patel-King, R. S., Rayburn, H. and Hynes, R. O. (1993). Defects in mesoderm, neural tube and vascular development in mouse embryos lacking fibronectin. *Development* **119**, 1079-1091.
George, E. L., Baldwin, H. S. and Hynes, R. O. (1997). Fibronectins are essential for heart and blood vessel morphogenesis but are dispensable for initial specification of precursor cells. *Blood* **90**, 3073-3081.
Gitler, A. D., Brown, C. B., Kochilas, L., Li, J. and Epstein, J. A. (2002). Neural crest migration and mouse models of congenital heart disease. *Cold Spring Harb. Symp. Quant. Biol.* **67**, 57-62.
Hallak, M. E. and Bongiovanni, G. (1997). Posttranslational arginylation of brain proteins. *Neurochem. Res.* **22**, 467-473.
Hayward, L. and Schwartz, R. (1986). Sequential expression of chicken actin genes during myogenesis. *J. Cell Biol.* **102**, 1485-1493.
Kaji, H., Novelli, G. D. and Kaji, A. (1963). A soluble amino acid-incorporating system from rat liver. *Biochim. Biophys. Acta* **76**, 474-477.
Karakozova, M., Kozak, M., Wong, C. C., Bailey, A. O., Yates, J. R., 3rd, Mogilner, A., Zebroski, H. and Kashina, A. (2006). Arginylation of beta-actin regulates actin cytoskeleton and cell motility. *Science* **313**, 192-196.
Kopitz, J., Rist, B. and Bohley, P. (1990). Post-translational arginylation of ornithine decarboxylase from rat hepatocytes. *Biochem. J.* **267**, 343-348.
Kwon, Y. T., Kashina, A. S. and Varshavsky, A. (1999). Alternative splicing results in differential expression, activity, and localization of the two forms of arginyl-tRNA-protein transferase, a component of the N-end rule pathway. *Mol. Cell. Biol.* **19**, 182-193.
Kwon, Y. T., Kashina, A. S., Davydov, I. V., Hu, R. G., An, J. Y., Seo, J. W., Du, F. and Varshavsky, A. (2002). An essential role of N-terminal arginylation in cardiovascular development. *Science* **297**, 96-99.
Lee, M. J., Tasaki, T., Moroi, K., An, J. Y., Kimura, S., Davydov, I. V. and Kwon, Y. T. (2005). RGS4 and RGS5 are in vivo substrates of the N-end rule pathway. *Proc. Natl. Acad. Sci. USA* **102**, 15030-15035.
LoRusso, S. M., Rhee, D., Sanger, J. M. and Sanger, J. W. (1997). Premyofibrils in spreading adult cardiomyocytes in tissue culture: evidence for reexpression of the embryonic program for myofibrillogenesis in adult cells. *Cell Motil. Cytoskeleton* **37**, 183-198.
Mai, W., Le Floc'h, J., Vray, D., Samarut, J., Barthez, P. and Janier, M. (2004). Evaluation of cardiovascular flow characteristics in the 129Sv mouse fetus using color-Doppler-guided spectral Doppler ultrasound. *Vet. Radiol. Ultrasound* **45**, 568-573.
Martin, A. F., Phillips, R. M., Kumar, A., Crawford, K., Abbas, Z., Lessard, J. L., de Tombe, P. and Solaro, R. J. (2002). Ca^{2+} activation and tension cost in myofilaments from mouse hearts ectopically expressing enteric gamma-actin. *Am. J. Physiol. Heart Circ. Physiol.* **283**, H642-H649.
Meng, H., Leddy, J. J., Frank, J., Holland, P. and Tuana, B. S. (1996). The association of cardiac dystrophin with myofibrils/Z-disc regions in cardiac muscle suggests a novel role in the contractile apparatus. *J. Biol. Chem.* **271**, 12364-12371.
Otey, C. A., Kalnoski, M. H., Lessard, J. L. and Bulinski, J. C. (1986). Immunolocalization of the gamma isoform of nonmuscle actin in cultured cells. *J. Cell Biol.* **102**, 1726-1737.
Otey, C. A., Kalnoski, M. H. and Bulinski, J. C. (1987). Identification and quantification of actin isoforms in vertebrate cells and tissues. *J. Cell. Biochem.* **34**, 113-124.
Otey, C. A., Kalnoski, M. H. and Bulinski, J. C. (1988). Immunolocalization of muscle and nonmuscle isoforms of actin in myogenic cells and adult skeletal muscle. *Cell Motil. Cytoskeleton* **9**, 337-348.
Otterbein, L. R., Graceffa, P. and Dominguez, R. (2001). The crystal structure of uncomplexed actin in the ADP state. *Science* **293**, 708-711.
Rai, R. and Kashina, A. (2005). Identification of mammalian arginyltransferases that modify a specific subset of protein substrates. *Proc. Natl. Acad. Sci. USA* **102**, 10123-10128.
Rai, R., Mushegian, A., Makarova, K. and Kashina, A. (2006). Molecular dissection of arginyltransferases guided by similarity to bacterial peptidoglycan synthases. *EMBO Rep.* **7**, 800-805.
Rhee, D., Sanger, J. M. and Sanger, J. W. (1994). The premyofibril: evidence for its role in myofibrillogenesis. *Cell Motil. Cytoskeleton* **28**, 1-24.
Rubenstein, P. A. and Spudich, J. A. (1977). Actin microheterogeneity in chick embryo fibroblasts. *Proc. Natl. Acad. Sci. USA* **74**, 120-123.
Sanger, J. W., Ayoob, J. C., Chowrashi, P., Zurawski, D. and Sanger, J. M. (2000). Assembly of myofibrils in cardiac muscle cells. *Adv. Exp. Med. Biol.* **481**, 89-102; discussion 103-105.
Sanger, J. W., Kang, S., Siebrands, C. C., Freeman, N., Du, A., Wang, J., Stout, A. L. and Sanger, J. M. (2005). How to build a myofibril. *J. Muscle Res. Cell Motil.* **26**, 343-354.
Sassoon, D., Garner, I. and Buckingham, M. (1988). Transcripts of alpha-cardiac and alpha-skeletal actins are early markers for myogenesis in the mouse embryo. *Development* **104**, 155-164.
Soffer, R. L. (1968). The arginine transfer reaction. *Biochim. Biophys. Acta* **155**, 228-240.
Takao, K. and Samejima, K. (1999). Arginyl-tRNA-protein transferase activities in crude supernatants of rat tissues. *Biol. Pharm. Bull.* **22**, 1007-1009.
Tullio, A. N., Accili, D., Ferrans, V. J., Yu, Z. X., Takeda, K., Grinberg, A., Westphal, H., Preston, Y. A. and Adelstein, R. S. (1997). Nonmuscle myosin II-B is required for normal development of the mouse heart. *Proc. Natl. Acad. Sci. USA* **94**, 12407-12412.
Vandekerckhove, J. and Weber, K. (1978). At least six different actins are expressed in a higher mammal: an analysis based on the amino acid sequence of the amino-terminal tryptic peptide. *J. Mol. Biol.* **126**, 783-802.
Wong, C. C. L., Xu, T., Rai, R., Bailey, A. O., Yates, J. R., Wolf, Y. I., Zebroski, H. and Kashina, A. (2007). Global analysis of posttranslational protein arginylation. *PLoS Biol.* **5**, e258.

gel_5_Oct06 #5570 RT: 48.27 AV: 1 NL: 2.74E3
T: ITMS + c ESI d Full ms2 785.16@cid35.00 [205.00-2000.00]

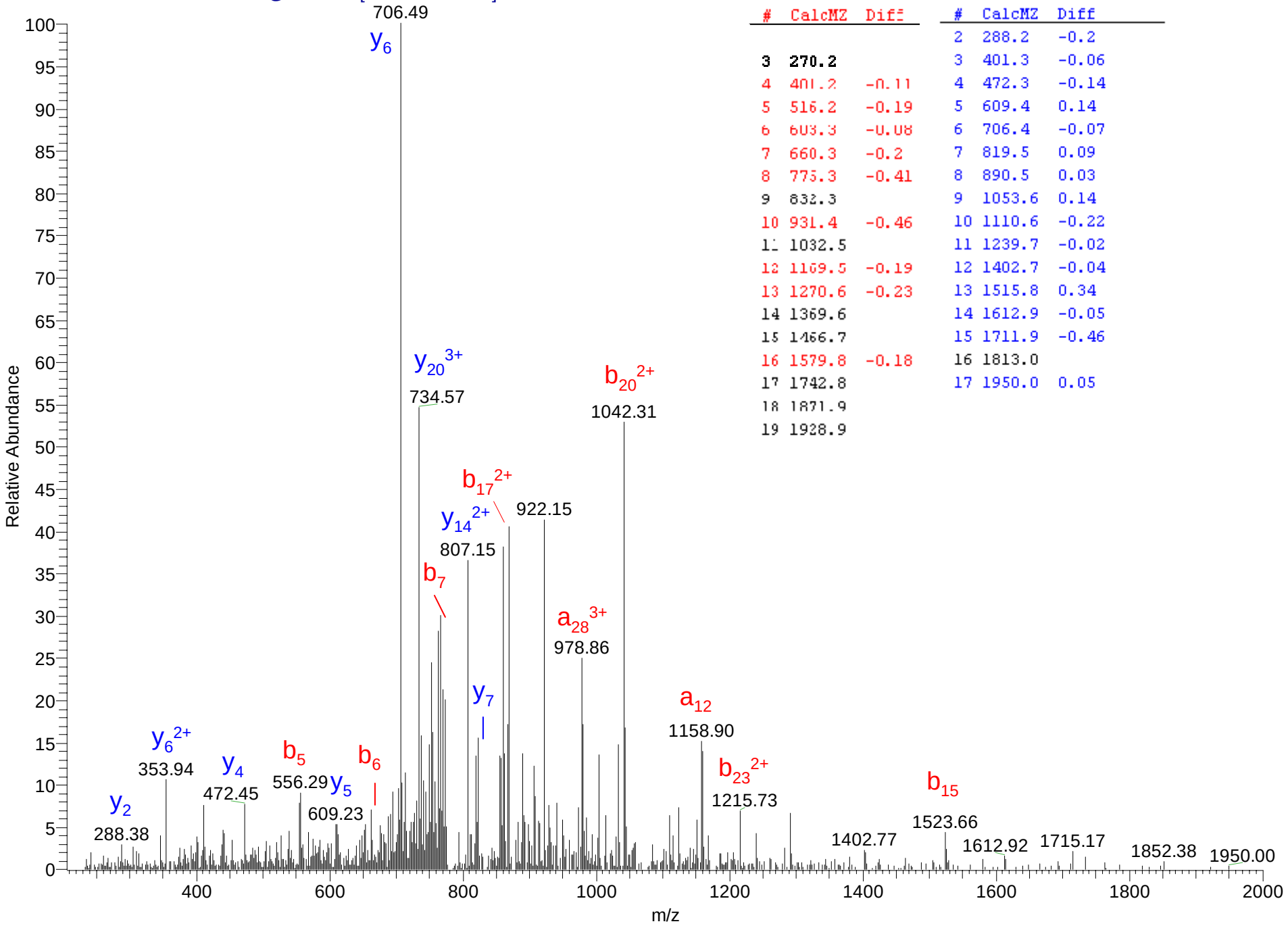

B +1			Y +1		
#	CalcMZ	Diff	#	CalcMZ	Diff
			2	288.2	-0.2
3	270.2		3	401.3	-0.06
4	401.2	-0.11	4	472.3	-0.14
5	516.2	-0.19	5	609.4	0.14
6	603.3	-0.08	6	706.4	-0.07
7	660.3	-0.2	7	819.5	0.09
8	775.3	-0.41	8	890.5	0.03
9	832.3		9	1053.6	0.14
10	931.4	-0.46	10	1110.6	-0.22
11	1032.5		11	1239.7	-0.02
12	1189.5	-0.19	12	1402.7	-0.04
13	1270.6	-0.23	13	1515.8	0.34
14	1369.6		14	1612.9	-0.05
15	1466.7		15	1711.9	-0.46
16	1579.8	-0.18	16	1813.0	
17	1742.8		17	1950.0	0.05
18	1871.9				
19	1928.9				

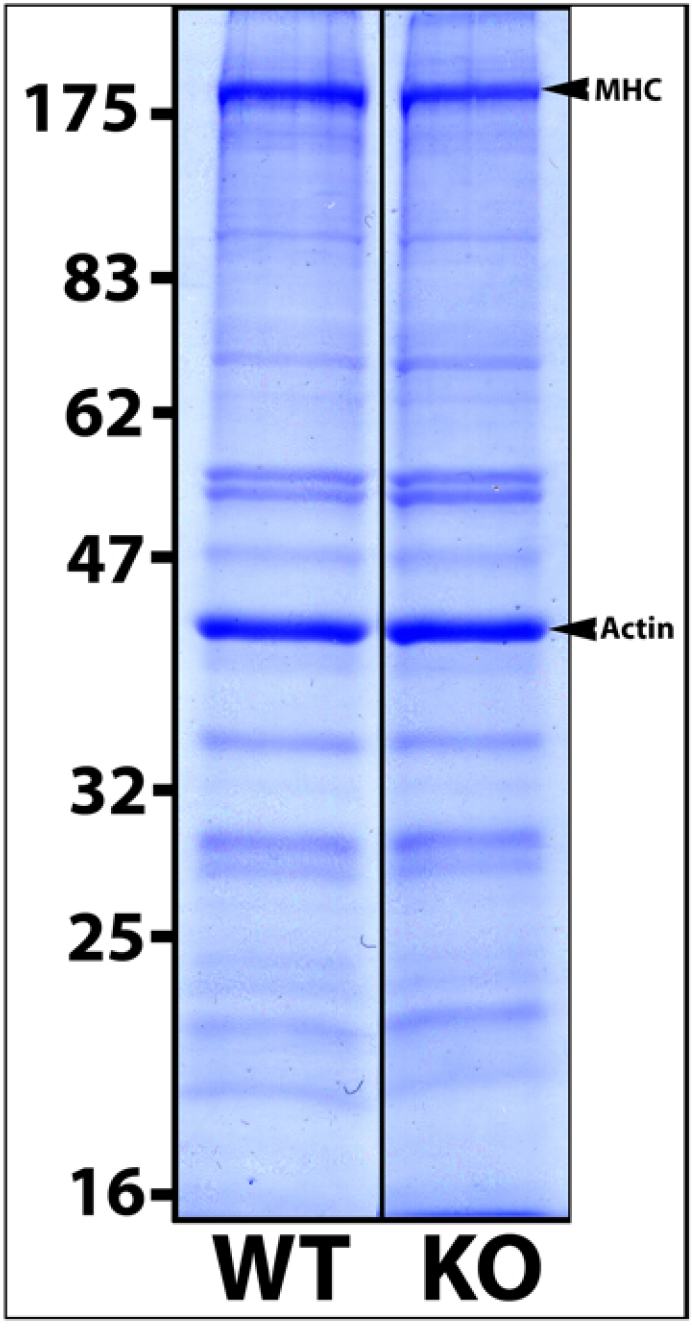

MHC:Actin ratio:

WT=0.94+/-0.07 (n=3)

KO=0.91+/-0.16 (n=4)

Actin distribution:

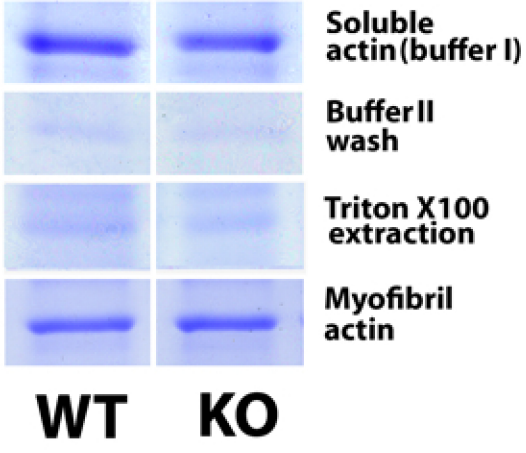

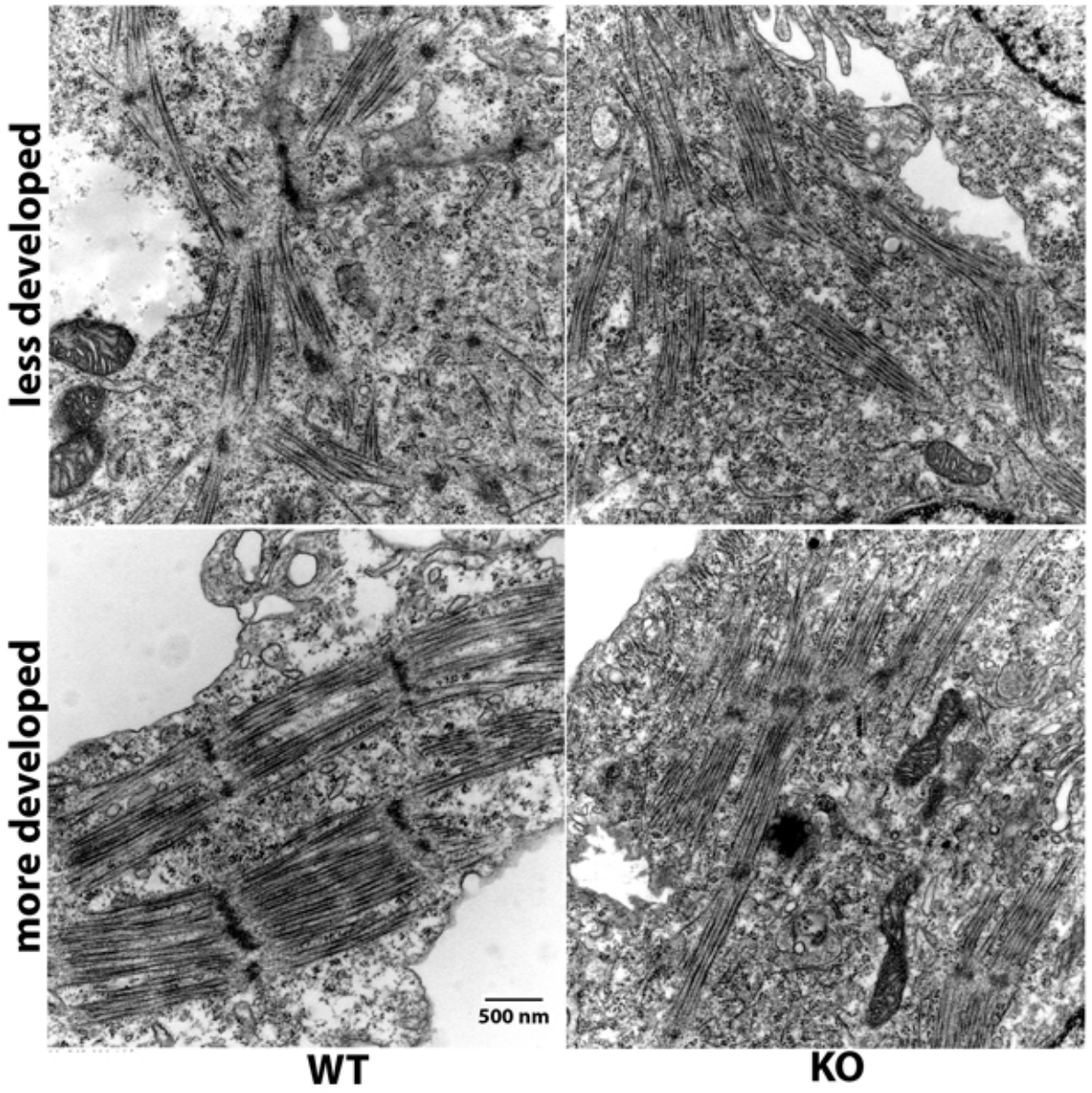
less developed
more developed
500 nm
WT
KO

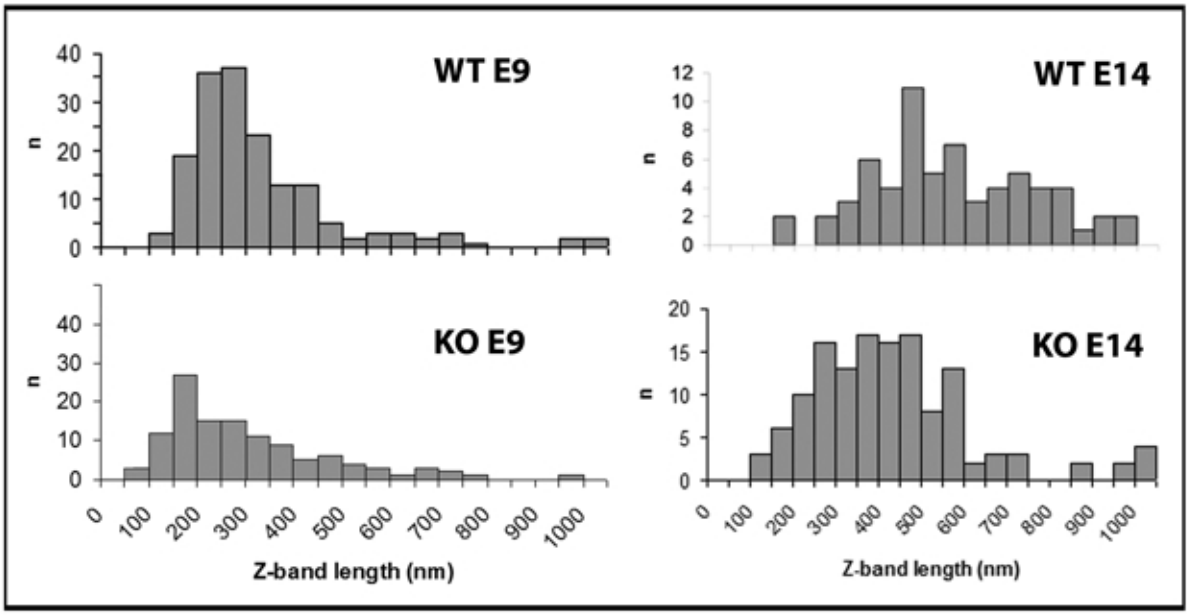
WT E9
KO E9
WT E14
KO E14
n
Z-band length (nm)

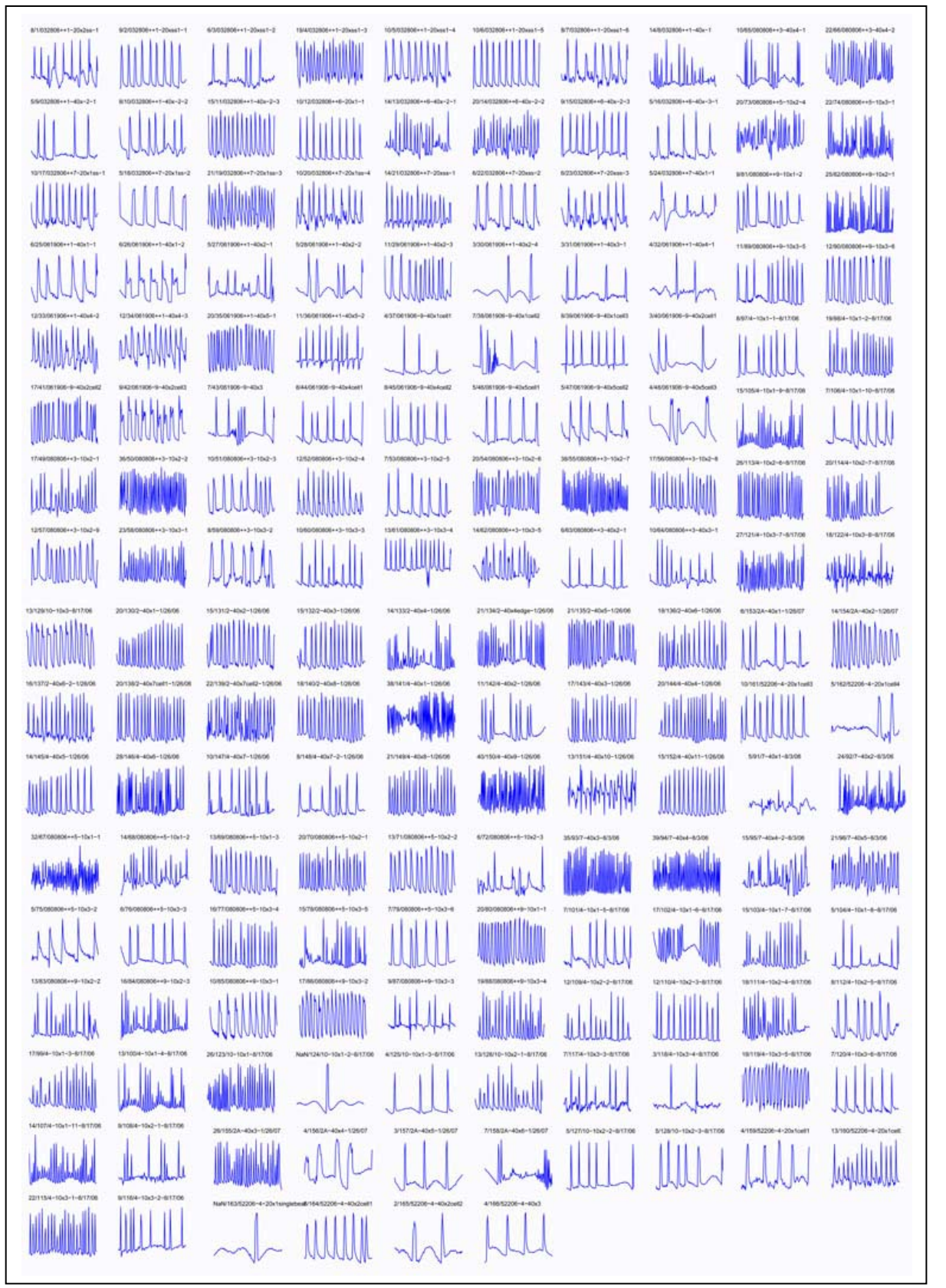
8/1/032806++1-20x2ss-1
9/2/032806++1-20xss1-1
6/3/032806++1-20xss1-2
19/4/032806++1-20xss1-3
10/5/032806++1-20xss1-4
10/6/032806++1-20xss1-5
8/7/032806++1-20xss1-6
14/8/032806++1-40x-1
10/65/080806++3-40x4-1
22/66/080806++3-40x4-2
5/9/032806++1-40x-2-1
8/10/032806++1-40x-2-2
15/11/032806++1-40x-2-3
10/12/032806++6-20x1-1
14/13/032806++6-40x-2-1
20/14/032806++6-40x-2-2
9/15/032806++6-40x-2-3
5/16/032806++6-40x-3-1
20/73/080808++5-10x2-4
22/74/080806++5-10x3-1
10/17/032806++7-20x1ss-1
5/18/032806++7-20x1ss-2
21/19/032806++7-20x1ss-3
10/20/032806++7-20x1ss-4
14/21/032806++7-20xss-1
8/22/032806++7-20xss-2
8/23/032806++7-20xss-3
5/24/032806++7-40x1-1
9/81/080806++9-10x1-2
25/82/080806++9-10x2-1
6/25/061906++1-40x1-1
6/26/061906++1-40x1-2
5/27/061906++1-40x2-1
5/28/061906++1-40x2-2
11/29/061906++1-40x2-3
3/30/061906++1-40x2-4
3/31/061906++1-40x3-1
4/32/061906++1-40x4-1
11/89/080806++9-10x3-5
12/90/080806++9-10x3-6
12/33/061906++1-40x4-2
12/34/061906++1-40x4-3
20/35/061906++1-40x5-1
11/36/061906++1-40x5-2
4/37/061906-9-40x1cell1
7/38/061906-9-40x1cell2
8/39/061906-9-40x1cell3
3/40/061906-9-40x2cell1
8/97/4-10x1-1-8/17/06
19/98/4-10x1-2-8/17/06
17/41/061906-9-40x2cell2
9/42/061906-9-40x2cell3
7/43/061906-9-40x3
8/44/061906-9-40x4cell1
8/45/061906-9-40x4cell2
5/46/061906-9-40x5cell1
5/47/061906-9-40x5cell2
4/48/061906-9-40x5cell3
15/105/4-10x1-9-8/17/06
7/106/4-10x1-10-8/17/06
17/49/080806++3-10x2-1
36/50/080806++3-10x2-2
10/51/080806++3-10x2-3
12/52/080806++3-10x2-4
7/53/080806++3-10x2-5
20/54/080806++3-10x2-6
39/55/080806++3-10x2-7
17/56/080806++3-10x2-8
26/113/4-10x2-6-8/17/06
20/114/4-10x2-7-8/17/06
12/57/080806++3-10x2-9
23/58/080806++3-10x3-1
8/59/080806++3-10x3-2
10/60/080806++3-10x3-3
13/61/080806++3-10x3-4
14/62/080806++3-10x3-5
6/63/080806++3-40x2-1
10/64/080806++3-40x3-1
27/121/4-10x3-7-8/17/06
18/122/4-10x3-8-8/17/06
13/129/10-10x3-8/17/06
20/130/2-40x1-1/26/06
15/131/2-40x2-1/26/06
15/132/2-40x3-1/26/06
14/133/2-40x4-1/26/06
21/134/2-40x4edge-1/26/06
21/135/2-40x5-1/26/06
18/136/2-40x6-1/26/06
8/153/2A-40x1-1/25/07
14/154/2A-40x2-1/26/07
16/137/2-40x6-2-1/26/06
20/138/2-40x7cell1-1/26/06
22/139/2-40x7cell2-1/26/06
18/140/2-40x8-1/26/06
38/141/4-40x1-1/26/06
11/142/4-40x2-1/26/06
17/143/4-40x3-1/26/06
20/144/4-40x4-1/26/06
10/161/52206-4-20x1cell3
5/162/52206-4-20x1cell4
14/145/4-40x5-1/26/06
28/146/4-40x6-1/26/06
10/147/4-40x7-1/26/06
8/148/4-40x7-2-1/26/06
21/149/4-40x8-1/26/06
40/150/4-40x9-1/26/06
13/151/4-40x10-1/26/06
15/152/4-40x11-1/26/06
5/91/7-40x1-8/3/06
24/92/7-40x2-8/3/06
32/67/080806++5-10x1-1
14/68/080806++5-10x1-2
13/69/080806++5-10x1-3
20/70/080806++5-10x2-1
13/71/080806++5-10x2-2
6/72/080806++5-10x2-3
35/93/7-40x3-8/3/06
39/94/7-40x4-8/3/06
15/95/7-40x4-2-8/3/06
21/96/7-40x5-8/3/06
5/75/080806++5-10x3-2
6/76/080806++5-10x3-3
16/77/080806++5-10x3-4
15/78/080806++5-10x3-5
7/79/080806++5-10x3-6
20/80/080806++9-10x1-1
7/101/4-10x1-5-8/17/06
17/102/4-10x1-6-8/17/06
15/103/4-10x1-7-8/17/06
5/104/4-10x1-8-8/17/06
13/83/080806++9-10x2-2
16/84/080806++9-10x2-3
10/85/080806++9-10x3-1
17/86/080806++9-10x3-2
9/87/080806++9-10x3-3
19/88/080806++9-10x3-4
12/109/4-10x2-2-8/17/06
12/110/4-10x2-3-8/17/06
18/111/4-10x2-4-8/17/06
8/112/4-10x2-5-8/17/06
17/99/4-10x1-3-8/17/06
13/100/4-10x1-4-8/17/06
26/123/10-10x1-8/17/06
NaN/124/10-10x1-2-8/17/06
4/125/10-10x1-3-8/17/06
13/126/10-10x2-1-8/17/06
7/117/4-10x3-3-8/17/06
3/118/4-10x3-4-8/17/06
18/119/4-10x3-5-8/17/06
7/120/4-10x3-6-8/17/06
14/107/4-10x1-11-8/17/06
9/108/4-10x2-1-8/17/06
26/155/2A-40x3-1/26/07
4/156/2A-40x4-1/26/07
3/157/2A-40x5-1/26/07
7/158/2A-40x6-1/26/07
5/127/10-10x2-2-8/17/06
5/128/10-10x2-3-8/17/06
4/159/52206-4-20x1cell1
13/160/52206-4-20x1cell
22/115/4-10x3-1-8/17/06
9/116/4-10x3-2-8/17/06
NaN/163/52206-4-20x1singlebeat
8/164/52206-4-40x2cell1
2/165/52206-4-40x2cell2
4/166/52206-4-40x3

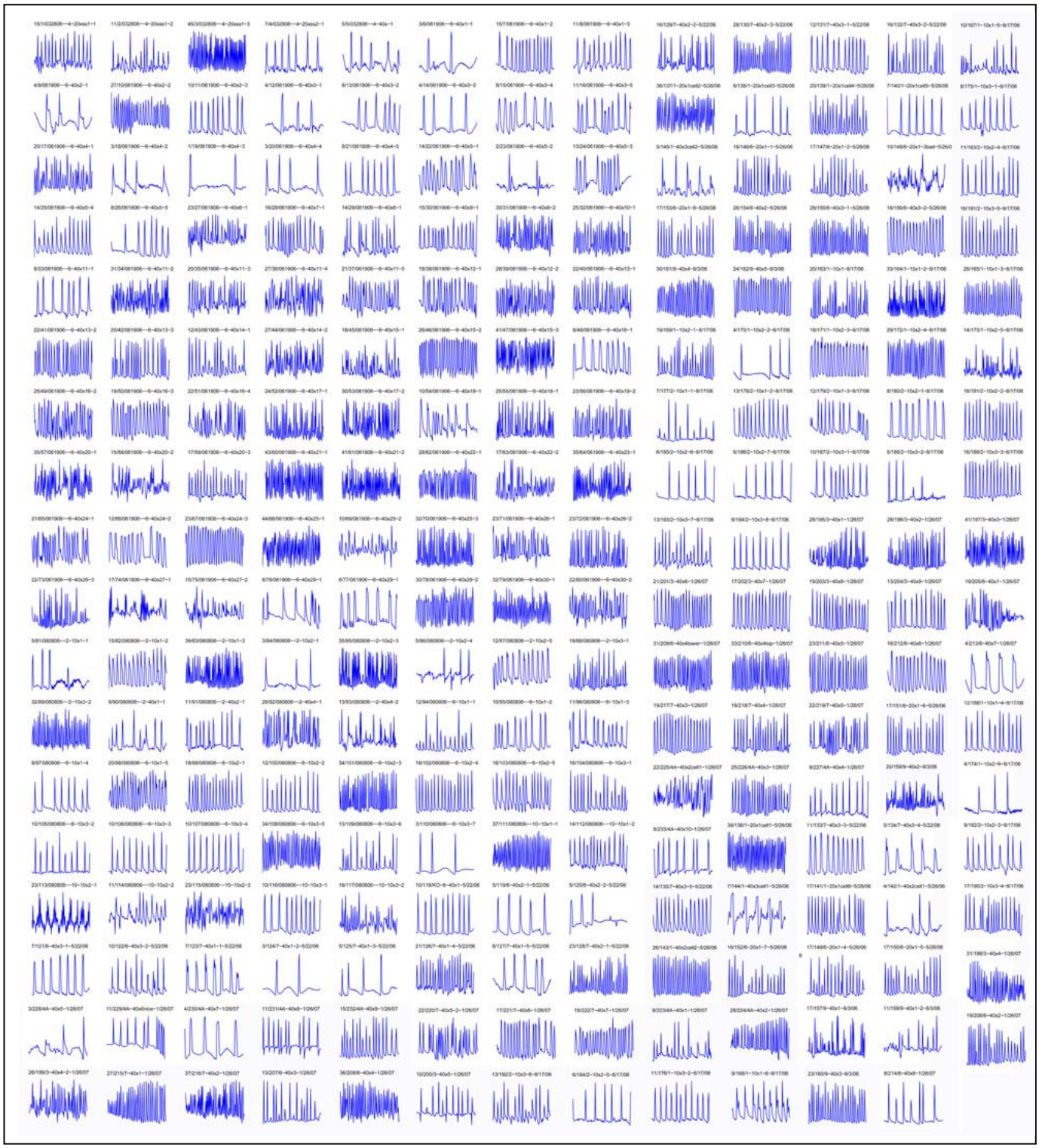

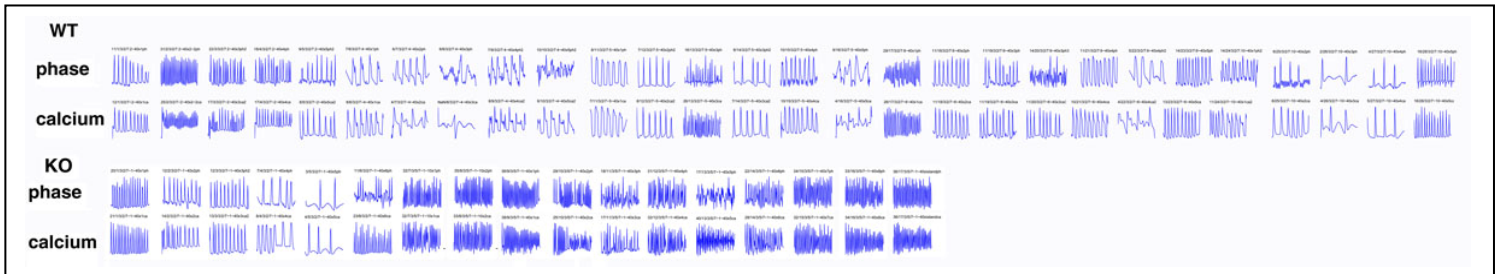
WT
phase
calcium
KO
phase
calcium